Eur. Phys. J. A **14**, 439–449 (2002)
DOI 10.1140/epja/i2002-10026-8

THE EUROPEAN PHYSICAL JOURNAL A

Spectroscopy of the deformed ^{125}Ce nucleus

C.M. Petrache[1,a], G. Lo Bianco[1], P.G. Bizzeti[2], A.M. Bizzeti-Sona[2], D. Bazzacco[3], S. Lunardi[3], M. Nespolo[3], G. de Angelis[4], P. Spolaore[4], N. Blasi[5], S. Brant[6], V. Krstić[6], and D. Vretenar[6]

[1] Dipartimento di Fisica, Università di Camerino and INFN, Sezione di Perugia, Italy
[2] Dipartimento di Fisica and INFN, Sezione di Firenze, Firenze, Italy
[3] Dipartimento di Fisica and INFN, Sezione di Padova, Padova, Italy
[4] INFN, Laboratori Nazionali di Legnaro, Legnaro, Italy
[5] INFN, Sezione di Milano, Milano, Italy
[6] Department of Physics, Faculty of Science, University of Zagreb, 10000 Zagreb, Croatia

Received: 19 February 2002 / Revised version: 22 March 2002
Communicated by C. Signorini

Abstract. The odd-even nucleus ^{125}Ce was studied via in-beam γ-ray spectroscopy using the ^{40}Ca + ^{92}Mo reaction at 190 MeV. Four rotational bands were observed, two of them being identified for the first time. New connecting transitions were identified between the bands, which leads to new spin assignment for one of the previously known bands. We propose $J = 7/2^-$ for the ground state of ^{125}Ce. The bands are discussed in the framework of the IBFM + broken-pairs model.

PACS. 23.20.Lv Gamma transitions and level energies – 21.10.Re Collective levels – 21.60.Ev Collective models – 27.60.+j $90 \leq A \leq 149$

1 Introduction

In order to investigate the variation of the level structure in the sequence of Ce nuclei when approaching the proton drip line, we have studied the ^{125}Ce nucleus in an experiment performed with the GASP array [1]. The ^{125}Ce nucleus is the lightest odd-even isotope in which band structures have been recently published by Paul *et al.* [2]. Two bands were reported: one built on the ground state proposed to have spin $5/2^+$ on the basis of the analysis of the β-delayed proton activity of ^{125}Ce [3], and with the first three γ-rays assigned previously by Osa *et al.* [4] from a study of the β^+/EC decay of ^{125}Pr; the other band, based on a $7/2^-$ state, was assigned to ^{125}Ce on the basis of the coincidence between the γ-rays and $A = 125$ recoils detected at the focal plane of a recoil mass separator. No γ-rays connecting the two bands were observed. In the heavier ^{127}Ce nucleus [5,6] three bands were identified: two built on $5/2^+$ and $7/2^-$ states as in ^{125}Ce, separated by an excitation energy estimated to be lower than 20 keV [6], and one based on a $1/2^+$ state, which is also present in the heavier ^{129,131,133}Ce nuclei [7,8]. Apparently, the excitation energy of the $7/2^-$ state with respect to the $5/2^+$ state decreases with decreasing neutron number. The ground state of the lighter Ce isotopes can thus have spin $7/2^-$, and not $5/2^+$ as proposed previously. It is important to establish the relative energy of the lowest excitations in an odd-even nucleus like ^{125}Ce, because one can estimate on this basis the deformation of the nucleus and from the comparison of the lowest excitations with the calculated energy of the orbitals close to the Fermi surface one can choose the best model to predict the nuclear behaviour at the limits of stability.

In the present paper we observe the previously known bands of ^{125}Ce up to much higher spins and excitation energy, and report two new rotational bands. The relative excitation of three of the four observed bands is also established. The observed structures are discussed in the framework of the interacting boson-fermion model plus broken pairs.

2 Experimental details

We populated high-spin states in ^{125}Ce using the ^{40}Ca + ^{92}Mo reaction, with a ^{40}Ca beam of 5 pnA intensity and an energy of 190 MeV. The beam was provided by the XTU Tandem accelerator of the Laboratori Nazionali di Legnaro. The target was a self-supporting ^{92}Mo foil with a thickness of 0.5 mg/cm^2. The experimental setup consisted of the GASP array for γ-ray detection and the ISIS ball for charged-particle detection [9].

The GASP array with 40 Compton-suppressed Ge detectors and the 80 element BGO ball was used for a γ^n

[a] e-mail: petrache@sunlb1.unicam.it

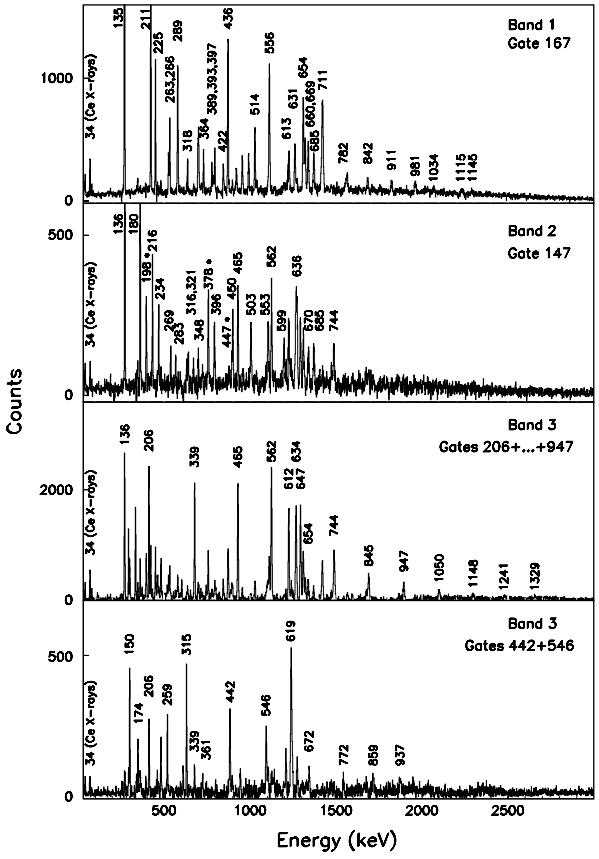

Fig. 1. Gamma spectra obtained from the $\alpha 2p$-gated matrix in coincidence with clean transitions of ^{125}Ce. The transitions marked with an asterix in the spectrum of band 2 are connecting transitions to band 3.

coincidence measurement. The experimental arrangement in GASP has been carefully prepared, in order to minimize the absorbtion of the low-energy X-rays. Light charged particles (p, d, t and α-particles) were detected with the ISIS ball, which is composed of 40 ΔE-E Si telescopes. Events were written on tape when two or more Ge detectors fired in coincidence with at least two BGO detectors. A total of 3.5×10^9 Compton-suppressed events have been collected.

The ^{125}Ce nucleus was populated via the $\alpha 2pn$ channel. The charged particles from each event were identified mainly as protons and α-particles and their energy measured. The events were then sorted according to the number of charged-particle detectors that fired in coincidence. For each charged-particle combination, *i.e.* $1p, 2p, 3p, 4p, \alpha p, \alpha 2p, 2\alpha, 2\alpha p$, E_γ-E_γ and E_γ-E_γ-E_γ matrices were produced off-line for further analysis. The level structure of ^{125}Ce has been derived mainly from the analysis of the $\alpha 2p$-gated data.

3 Results

Coincidence spectra showing transitions of the four bands assigned to ^{125}Ce are given in fig. 1. They are obtained from the $\alpha 2p$ matrix by gating on clean γ-rays, selected in order to show the majority of transitions in the band: the 167 keV transition for band 1, the 147 keV transition for band 2, and two sums of selected gates (206, 339, 465, 562, 634, 647, 612, 654, 744, 845, 947 keV and 442, 546 keV) for band 3.

The decay scheme of ^{125}Ce resulting from the present analysis is shown in fig. 2. The spins of the levels have been inferred (when possible) from a directional correlation orientation (DCO) analysis as described, *e.g.*, in [10]. Information about the observed transitions are given in table 1. In fig. 3 we have drawn the $B(M1)/B(E2)$ branching ratios for the three bands consisting of mixed $M1/E2$ dipole and cross-over $E2$ transitions, assuming that the mixing ratios of the dipole $M1/E2$ transitions is zero.

The level scheme of ^{125}Ce presented in this work is constructed starting from the previously reported [2] low-lying levels in bands 1 and 2. We confirm the transitions assigned to band 1 up to the 710 and 631 keV transitions of the sequences built on the $7/2^-$ and $9/2^-$ states, respectively. On top of each of these two sequences of transitions we add six and seven new transitions, respectively, with assigned quadrupole character (see fig. 2 and table 1). Ten new dipole transitions were also observed to connect the levels of band 1. To this band is assigned a $\nu h_{11/2}[523]7/2^-$ configuration based on the signature splitting and alignment properties, and was observed at low excitation energy in many odd-even Ba, Ce and Nd nuclei in this mass region.

The transitions previously assigned to band 2 are confirmed, with the exception of the 465 keV transition, which we assign to band 3 (see below). We extend the band up to spin $(29/2^+)$ by adding seven new quadrupole transitions and six dipole transitions. We establish also a transition of 283 keV in parallel with the 147 and 136 keV transitions. To this band was assigned a $\nu d_{5/2}[402]5/2^+$ configuration, based on its vanishingly small signature splitting.

Band 3 is completely new, being as well populated as band 2. The $\nu d_{3/2}[411]1/2^+$ configuration assignment to this band is consistent with the sistematics [6–8] and is based on branching ratios and signature splitting arguments. The assigned spins to this band are such that the band head spin is 1/2, as expected for the $\nu d_{3/2}[411]1/2^+$ configuration. We also identified connecting transitions with band 2, which were essential in deducing the relative energy and spins of the two bands. All these connecting transitions are weak and only in one case, the 378 keV $11/2^+ \rightarrow 7/2^+$ transition, we could extract the DCO ratio, which is 0.92(26). This value is compatible with either quadrupole or mixed $M1/E2$ transitions. However, one can safely exclude the mixed $M1/E2$ character on the basis of the following arguments. If the 378 keV transiton would have a mixed $M1/E2$ character, one would obtain spins $9/2^+$ and $13/2^+$ for the levels of band 2 connected by the 396 keV transition of stretched $E2$ character. The inter-band 357 keV transition would be a $13/2^+ \rightarrow 7/2^+$ $M3$ transition, leading to a half-life for the $13/2^+$ level of band 2 of the order of $\sim$ 0.1 s, which is in contradiction with the experimental data. The only choice for

Table 1. Gamma-ray energies, intensities and DCO ratios for transitions in ^{125}Ce.

E_γ (keV)[a]	Trans. intens.[b]	DCO ratios[c]	Assign. $I_i^\pi \to I_f^\pi$
55.7	0.6(2)		$7/2^+ \to 5/2^+$
79.4	< 0.2		$11/2^+ \to 9/2^+$
93.8	5(1)	0.76(20)[q]	$(9/2^-) \to (7/2^-)$
134.6	104(4)	0.59(4)[q]	$(9/2^-) \to (7/2^-)$
135.5	45(2)	0.83(33)[q]	$5/2^+ \to (7/2^-)$
146.5	29(1)	0.73(15)[q]	$7/2^+ \to 5/2^+$
149.8	9.4(5)	0.86(28)[q]	$5/2^+ \to 3/2^+$
166.6	100(2)	0.48(6)[q]	$(11/2^-) \to (9/2^-)$
173.1	12.0(6)	0.28(11)[q]	$(11/2^-) \to (9/2^-)$
173.7	4.8(1.6)	0.92(36)[q]	$5/2^+ \to 1/2^+$
180.3	26(1)	0.52(9)[q]	$9/2^+ \to 7/2^+$
186.2	1.4(1)		$7/2^+ \to 5/2^+$
198.0	6.6(7)		$11/2^+ \to 9/2^+$
205.6	20.4(8)	1.09(13)[q]	$7/2^+ \to 3/2^+$
211.2	46(1)	0.48(6)[q]	$(13/2^-) \to (11/2^-)$
212.5	0.8(2)		$15/2^+ \to 13/2^+$
215.8	9.2(5)	0.48(20)[q]	$11/2^+ \to 9/2^+$
224.6	22(1)	0.46(4)[q]	$(15/2^-) \to (13/2^-)$
234.2	6.2(7)	0.43(14)[q]	$13/2^+ \to 11/2^+$
259.2	4.0(4)	0.87(26)[q]	$9/2^+ \to 7/2^+$
262.7	5.2(3)	0.67(11)[q]	$(31/2^-) \to (29/2^-)$
266.1	9.0(4)	0.45(6)[q]	$(19/2^-) \to (17/2^-)$
269.2	4.0(6)	0.55(14)[q]	$15/2^+ \to 13/2^+$
282.7	3.2(7)		$7/2^+ \to (7/2^-)$
283.3	3.0(7)	0.38(17)[q]	$17/2^+ \to 15/2^+$
287.8	4.8(8)		$(27/2^-) \to (25/2^-)$
289.4	16(2)	0.49(8)[q]	$(17/2^-) \to (15/2^-)$
289.9	5.4(8)		$(23/2^-) \to (21/2^-)$
301.2	27(2)	0.96(20)[q]	$(11/2^-) \to (7/2^-)$
315.0	7.8(7)	0.95(20)[q]	$9/2^+ \to 5/2^+$
315.5	3.4(6)	0.54(20)[q]	$19/2^+ \to 17/2^+$
318.0	4.6(6)	0.43(17)[q]	$(35/2^-) \to (33/2^-)$
320.5	4.0(6)	0.57(36)[q]	$21/2^+ \to 19/2^+$
326.6	9(1)		$9/2^+ \to 5/2^+$
337	2.8(3)		$25/2^+ \to 23/2^+$
338.6	31(1)	0.93(15)[q]	$11/2^+ \to 7/2^+$
348	4(1)		$23/2^+ \to 21/2^+$
351	4.8(5)	0.54(17)[q]	$(33/2^-) \to (31/2^-)$
356.6	3.4(3)		$11/2^+ \to 7/2^+$
361.4	2.8(5)		$13/2^+ \to 11/2^+$
364.4	6.2(7)	0.51(14)[q]	$(21/2^-) \to (19/2^-)$
377.7	30.4(8)	0.97(14)[q]	$(13/2^-) \to (9/2^-)$
378.3	10(1)	0.92(26)[q]	$11/2^+ \to 7/2^+$
388.9	4.0(2)		$(39/2^-) \to (37/2^-)$
392.9	2.4(2)		$(37/2^-) \to (35/2^-)$
396.1	10.4(9)	0.98(31)[q]	$11/2^+ \to 7/2^+$
397.1	6.6(3)	0.46(9)[q]	$(29/2^-) \to (27/2^-)$
422.0	4.8(6)	0.60(15)[q]	$(25/2^-) \to (23/2^-)$
435.9	32(4)	1.01(10)[q]	$(15/2^-) \to (11/2^-)$
441.5	12.2(6)	1.26(26)[q]	$13/2^+ \to 9/2^+$
443.5	1.0(2)		$17/2^+ \to 15/2^+$
446.9	3.4(5)		$15/2^+ \to 11/2^+$
449.7	10.2(8)	1.02(35)[q]	$13/2^+ \to 9/2^+$
464.6	28.0(9)	0.98(9)[q]	$15/2^+ \to 11/2^+$
479.1	10.0(1)	1.00(53)[q]	$(15/2^-) \to (11/2^-)$
502.7	11.6(7)	0.96(25)[q]	$15/2^+ \to 11/2^+$
514.0	23(1)	0.98(15)[q]	$(17/2^-) \to (13/2^-)$
546.4	12(1)	0.96(24)[q]	$17/2^+ \to 13/2^+$
552.6	14(1)		$17/2^+ \to 13/2^+$
555.6	34(2)	1.00(10)[q]	$(19/2^-) \to (15/2^-)$
562.1	27(2)	1.09(11)[q]	$19/2^+ \to 15/2^+$
598.8	10.6(8)		$19/2^+ \to 15/2^+$
612.4	15.8(6)	0.90(15)[q]	$31/2^+ \to 27/2^+$
613.0	11(1)		$(33/2^-) \to (29/2^-)$
613.9	9.9(7)	0.88(44)[q]	$(19/2^-) \to (15/2^-)$
619.2	10(1)	0.96(21)[q]	$21/2^+ \to 17/2^+$
619.2	8(1)	0.96(21)[q]	$25/2^+ \to 21/2^+$
630.5	14(1)	1.08(14)[q]	$(21/2^-) \to (17/2^-)$
633.5	23.6(6)	1.04(15)[q]	$23/2^+ \to 19/2^+$
636.3	14(2)		$21/2^+ \to 17/2^+$
646.8	18.6(6)	0.97(12)[q]	$27/2^+ \to 23/2^+$
654.2	11.6(8)	1.00(10)[q]	$35/2^+ \to 31/2^+$
654.4	30(2)	1.00(10)[q]	$(23/2^+) \to (19/2^+)$
660.2	17.0(5)	1.10(13)[q]	$(31/2^-) \to (27/2^-)$
668.5	16.8(5)	0.97(17)[q]	$(35/2^-) \to (31/2^-)$
670.0	11.6(8)	1.04(30)[q]	$23/2^+ \to 19/2^+$
671.6	3.0(5)	1.12(32)[sq]	$29/2^+ \to 25/2^+$
684.9	15(2)	0.84(21)[q]	$25/2^+ \to 21/2^+$
685.1	12.6(7)	0.83(18)[sq]	$(29/2^-) \to (25/2^-)$
710	24(4)		$(27/2^-) \to (23/2^-)$
711	8(2)		$(37/2^-) \to (33/2^-)$
712	12(3)		$(25/2^-) \to (21/2^-)$
723.8	7.0(6)		$(23/2^-) \to (19/2^-)$
744	14(2)		$(29/2^+) \to 25/2^+$
744.4	9.2(6)	1.02(35)[q]	$39/2^+ \to 35/2^+$
771.8	1.9(3)		$(33/2^+) \to 29/2^+$
781.9	9(1)		$(39/2^-) \to (35/2^-)$
817.0	5.0(6)		$(27/2^-) \to (23/2^-)$
841.7	6.2(6)		$(41/2^-) \to (37/2^-)$
844.6	6.2(4)	1.06(18)[sq]	$43/2^+ \to 39/2^+$
858.8	1.5(5)		$(37/2^+) \to (33/2^+)$
900.1	4.0(3)		$(31/2^-) \to (27/2^-)$
910.9	5.4(8)		$(43/2^-) \to (39/2^-)$
936.7	1.3(5)		$(41/2^+) \to (37/2^+)$
947.2	4.2(4)	0.88(36)[q]	$47/2^+ \to 43/2^+$
977	3.6(6)		$(35/2^-) \to (31/2^-)$
980.5	5.8(7)		$(45/2^-) \to (41/2^-)$
1034.4	2.6(6)		$(47/2^-) \to (43/2^-)$
1049.6	2.4(4)		$(51/2^+) \to 47/2^+$
1065.6	2.6(5)		$(39/2^-) \to (35/2^-)$
1115	2.2(6)		$(49/2^-) \to (45/2^-)$
1145	2.0(6)		$(51/2^-) \to (47/2^-)$
1148	1.0(2)		$(55/2^+) \to (51/2^+)$
1171	2.5(5)		$(43/2^-) \to (39/2^-)$
1241	< 1		$(59/2^+) \to (55/2^+)$
1295	1.9(4)		$(47/2^-) \to (43/2^-)$
1329	< 0.5		$(63/2^+) \to (59/2^+)$

[a] The error on the transition energies is 0.2 keV for transitions below 1000 keV and intensities larger that 5% of the ^{125}Ce channel, 0.5 keV for transitions above 1000 keV and intensities lower than 5%, and 1 keV for transitions above 1200 keV and/or weaker than 1%.

[b] Relative intensities corrected for efficiency. The transition intensities were obtained from a combination of total projection and gated spectra.

[c] The DCO ratios have been deduced from an asymmetric $\gamma\gamma$ coincidence matrix gated by the αp combination of charged particles detected by the isotropic ISIS ball. The tentative spin-parity of the states are given in parentheses.

[q] Gated by a "stretched" quadrupole transition.

[sq] Gated by a sum "stretched" quadrupole transition.

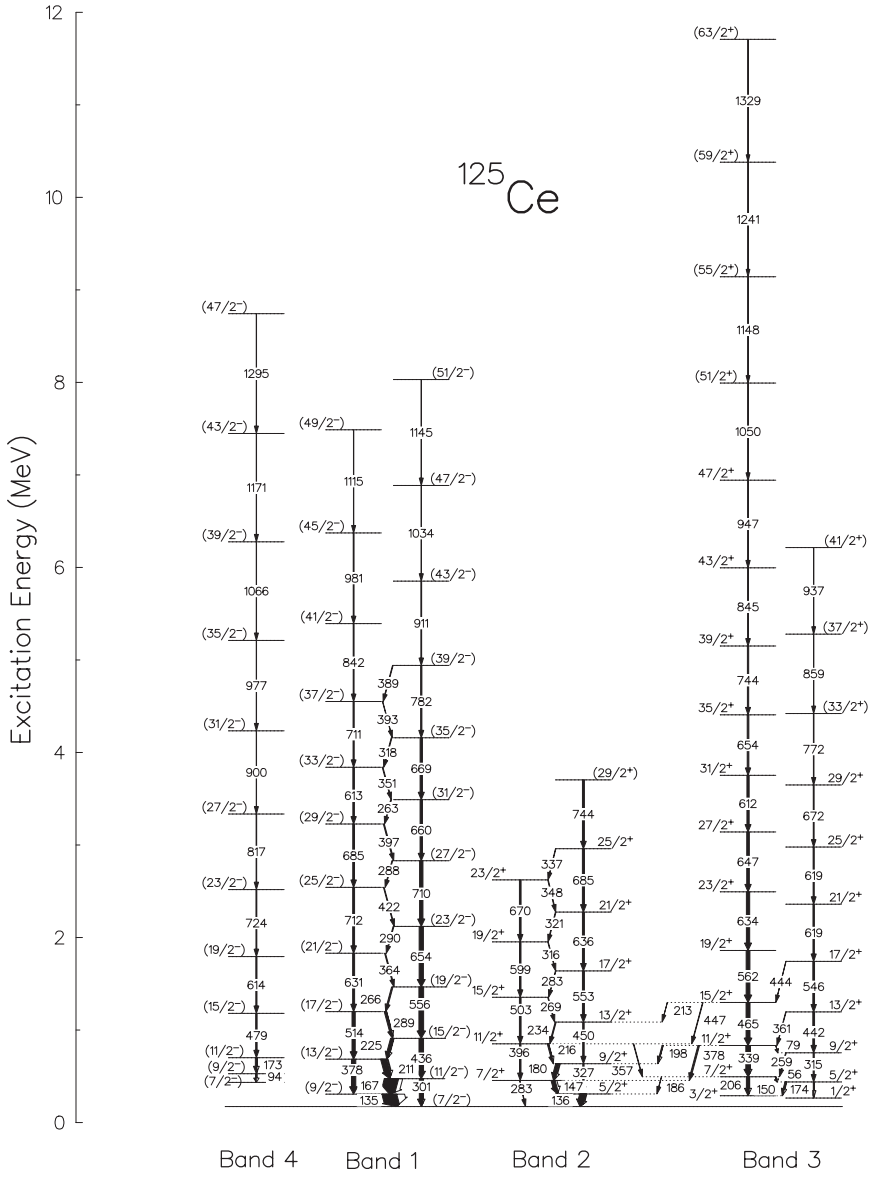

Fig. 2. Level scheme of ^{125}Ce deduced from the present work. The transition intensities are proportional to the width of the arrows.

the electromagnetic character of the inter-band 378 keV transition is the stretched $E2$, which determines the relative spins of bands 2 and 3. The spins we assign to the states of band 2 are one unit lower than previously proposed in ref. [2], which implies that the band head spin $5/2^+$ is assigned to the state populated by the 147 keV transition. The band then decays through the 136 keV and the 283 keV transitions to a level with a different configuration. Although the DCO ratio for the 136 keV transition would be consistent with the $M1/E2$ character, no other positive-parity configurations are expected at low excitation energy. The error on the DCO ratio is such that a pure dipole cannot be excluded. If the $E1$ character is assumed for this transition, the level populated by this and the 283 keV transition could have spin and parity $5/2^-$ or $7/2^-$. The band heads of the bands [523]$7/2^-$ and [402]$5/2^+$ lie close in excitation energy in this mass region, the former becoming lower as deformation increases. In heavier nuclei, with smaller deformation, the $7/2^-$ state is observed to decay to the $5/2^+$ state. In the present work, band 1 is the most intense, in agreement with the previous observation by Paul *et al.* [2], suggesting it to be the ground-state band. As already mentioned in the introduction, the spin assigned tentatively to the ground state of ^{125}Ce is $5/2^+$, being based on the analysis of the β-delayed proton activity into states of ^{124}Ba [3]. However, one expects the $7/2^-$ and $5/2^+$ states in the light Ce nuclei to be very close in energy, and to find the $7/2^-$ state below the $5/2^+$ state for large deformation [11]. On the basis of the observed band structures in ^{125}Ce and on the systematics of the relative energy of the $7/2^-$ and $5/2^+$ bands observed in the heavier odd-even Ce nuclei,

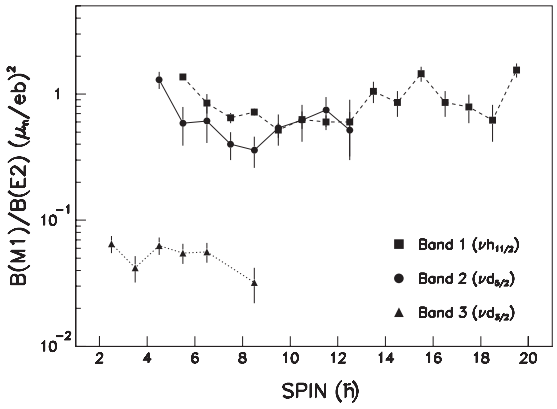

Fig. 3. Experimental branching ratios for the bands observed in ^{125}Ce.

we assign the $7/2^-$ state as the ground state of ^{125}Ce. This choice is in general agreement with the population pattern of the various observed bands in ^{125}Ce. It gives also a good explanation for the non-observation of the decay from the $3/2^+$ and $1/2^+$ states of band 3 to the $7/2^-$ state, the difference in spin-parity between the states leading to very prohibited $M2$ or $E3$ transitions.

Band 4 is observed here for the first time. It consists of two dipole transitions of 94 and 173 keV (most probably having a mixed $M1/E2$ character) on top of which we placed nine quadrupole transitions. This band feeds into low-lying levels of band 1 by means of connecting transitions that we could not identify. We will not discuss this band in detail in the present work. We assigned tentative spins and negative parity to the observed states, assuming a $h_{9/2}/f_{7/2}$ intruder configuration, which was also identified in various well-deformed neighboring nuclei.

4 Interacting boson fermion plus broken-pairs model analysis of the level structure of ^{125}Ce

The theoretical analysis of low and high angular-momentum states in ^{125}Ce is performed with the Interacting Boson Fermion plus Broken-Pairs Model (IBFBPM) [12–15], which is based on the IBM/IBFM framework [16–19], and can be applied in the description of excitation spectra and electromagnetic properties of states with angular momentum $I \leq 30\,\hbar$. In order to describe states with relatively high angular momentum, the IBM/IBFM model space has to be extended by including part of the original shell model fermion space through successive breaking of correlated S and D pairs (s- and d-bosons).

The approach is based on the simplest version of the IBM/IBFM models: the boson space consists of s- and d-bosons, no distinction is made between proton and neutron bosons. High-spin states are generated not only by the alignment of d-bosons, but also by coupling fermion pairs to the boson core. A boson can be destroyed, *i.e.* a correlated fermion pair can be broken by the Coriolis interaction and the resulting non-collective fermion pair

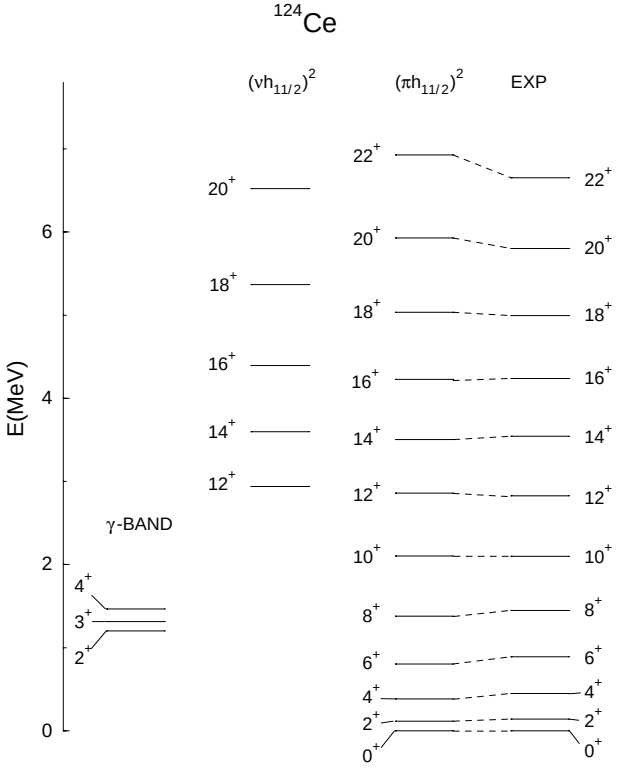

Fig. 4. Positive-parity states in the nucleus ^{124}Ce compared with the results of the IBFBPM calculation. Only the yrast band was observed experimentally [20].

recouples to the core. The structure of high-spin states is therefore determined by broken pairs. This framework has been very successfully applied in the analysis of high-spin structures in even-even and odd-even nuclei in the Hg, Sr-Zr, Cd and Nd-Sm regions.

The model space for an odd-even nucleus with $2N+1$ valence nucleons reads

$$|(N)\text{ bosons} \otimes 1\text{ fermion}\rangle \;\oplus$$
$$|(N-1)\text{ bosons} \otimes 1\text{ broken pair} \otimes 1\text{ fermion}\rangle.$$

The two fermions in the broken pair can be of the same type as the unpaired fermion, resulting in a space with three identical fermions. If the fermions in the broken pair are different from the unpaired one, the fermion basis contains two protons and one neutron or vice versa.

The model Hamiltonian contains four basic terms: the IBM-1 boson Hamiltonian [17], the fermion Hamiltonian, the boson-fermion interactions of IBFM-1 [19], and a pair breaking interaction that mixes states with different number of fermions [12].

If the three-fermion basis consists of proton and neutron states (the broken-pair nucleons and the odd nucleon are of different type), there will be two boson-fermion interaction terms in the Hamiltonian. Most of the parameters of the model Hamiltonian are taken from analyses of low- and high-spin states in neighboring even- and odd-A nuclei. Only a minimal number of model parameters are adjusted to the high-spin structure of a specific nucleus.

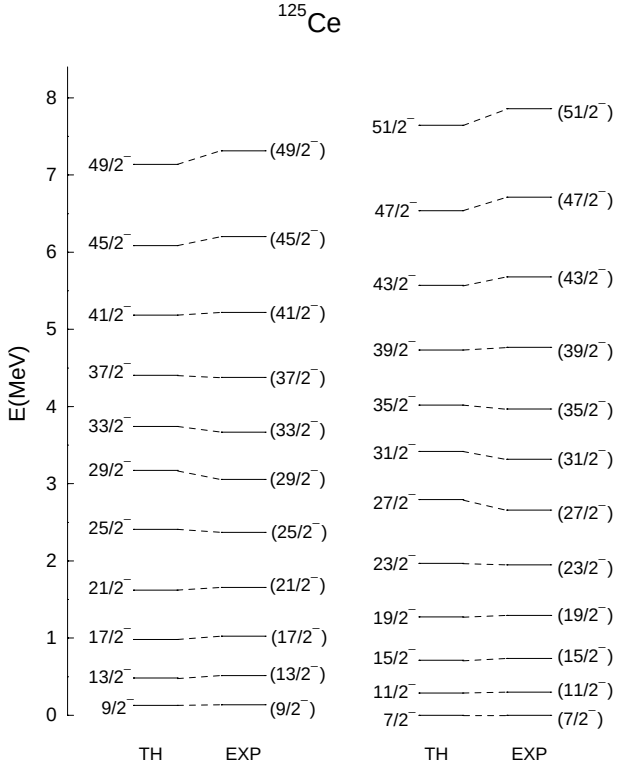

Fig. 5. The negative-parity states of band 1 in ^{125}Ce compared with the results of the IBFBPM calculation.

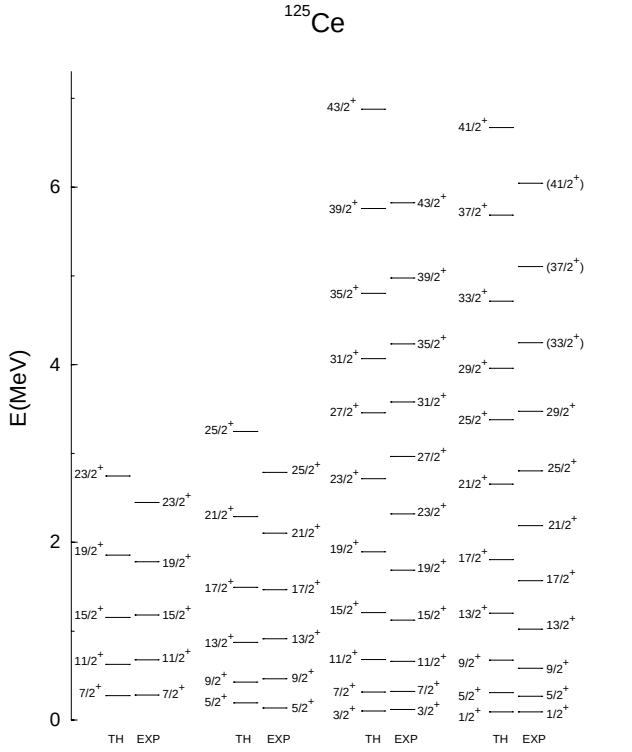

Fig. 6. The positive-parity states of bands 2 and 3 in ^{125}Ce compared with the results of the IBFBPM calculation.

The core nucleus for ^{125}Ce is ^{124}Ce [20]. This nucleus displays a transitional structure between deformed nuclei (lighter Ce isotopes) described by the $SU(3)$ limit of the IBM, and γ-soft nuclei (heavier Ce isotopes) which correspond to the $O(6)$ limit of the IBM. The $SU(3)$-$O(6)$ transition can be described by the boson Hamiltonian

$$H_{\rm IBM} = -\frac{\alpha}{10}\, Q\cdot Q \;+\; \frac{\beta}{10}\, L\cdot L\,, \qquad (1)$$

and is determined by the value of the parameter χ in the quadrupole boson operator [17]. The limiting cases are: $\chi = 0$ which corresponds to the $O(6)$ limit of the IBM-1, and $\chi = -\frac{\sqrt{7}}{2}$ which describes a prolate shape in the $SU(3)$ dynamical symmetry limit. The parameters of the collective Hamiltonian have been adjusted in the recent analysis of the odd-odd nucleus ^{126}Pr [21], for which ^{124}Ce was also used as the core nucleus: $\alpha = 0.19$ MeV, $\beta = 0.13$ MeV, $\chi = -1.0$ and the boson number $N = 12$. These values are very close to the ones used for ^{126}Ce [22]: $\alpha = 0.19$ MeV, $\beta = 0.16$ MeV, $\chi = -0.85$, $N = 11$. The ^{124}Ce nucleus is more deformed and thus a larger absolute value of χ is necessary. The value $\chi = -1.0$ is consistently used in the boson operator of the fermion-boson quadrupole interaction (both for protons and neutrons), as well as in the $E2$ boson operator.

The empirical systematics of high-spin structures in neighboring nuclei, as well as theoretical analyses, indicate that the only important proton contribution to the wave functions of the high-spin states close to the yrast line in ^{124}Ce and ^{125}Ce comes from the unique-parity orbital $\pi h_{11/2}$. The occupation probability $v^2(\pi h_{11/2}) = 0.06$ is calculated in the BCS approximation with Kisslinger-Sorensen single-proton energies [23], and $G = \frac{23}{A}$ MeV for the strength of the pairing interaction. The resulting quasiparticle energy is reduced by 300 keV to the value $\varepsilon(\pi h_{11/2}) = 1.70$ MeV. This modification is required by the experimental position of the 12_1^+ state in ^{124}Ce [20].

The parameterization of neutron particle energies for ^{126}Pr in ref. [21] was based on data from ref. [24]. In the present analysis an improved parameterization, based on new experimental data on ^{125}Ce, is used for the neutron particle energies E: $E(d_{5/2}) = 0$ MeV, $E(g_{7/2}) = 0.05$ MeV, $E(h_{11/2}) = 1.15$ MeV, $E(s_{1/2}) = 1.55$ MeV and $E(d_{3/2}) = 1.9$ MeV. In a BCS calculation with $G = \frac{23}{A}$ MeV for the strength of the pairing interaction, the following values of neutron quasiparticle energies and occupation probabilities are obtained: $\varepsilon(\nu h_{11/2}) = 1.32$ MeV, $\varepsilon(\nu s_{1/2}) = 1.46$ MeV, $\varepsilon(\nu g_{7/2}) = 1.55$ MeV, $\varepsilon(\nu d_{5/2}) = 1.58$ MeV, $\varepsilon(\nu d_{3/2}) = 1.65$ MeV, $\varepsilon(\nu f_{7/2}) = 5.32$ MeV, $v^2(\nu h_{11/2}) = 0.40$, $v^2(\nu s_{1/2}) = 0.27$, $v^2(\nu g_{7/2}) = 0.77$, $v^2(\nu d_{5/2}) = 0.78$, $v^2(\nu d_{3/2}) = 0.19$ and $v^2(\nu f_{7/2}) = 0.01$. A discussion on the role of the $\nu f_{7/2}$ orbital in the high-spin structure of this mass region can be found in ref. [21].

The experimental yrast sequence of states in ^{124}Ce is compared with the calculated spectrum in fig. 4. The strength parameters of the fermion-boson interactions are the same as the ones in our calculation of the nucleus ^{126}Ce [22]. The calculation is performed in a configuration space of boson states, states based on one proton pair and states based on one neutron pair. For $I \leq 10^+$ the

Table 2. Electromagnetic transition properties of states in ^{125}Ce. In the first column the transition is denoted by its initial and final angular momentum and parity assignments I_k^π. The index k is the label of the band. In the second and third columns the calculated B(E2) and B(M1) values are shown, respectively. The experimental and IBFBPM γ-intensities are compared in the last two columns. Only those unobserved transitions with calculated intensity $> 3\%$ of the main branch are included.

Transition	IBFBPM		I_γ	
	$B(E2)$ (e^2b^2)	$B(M1)$ (μ_N^2)	Exp.	IBFBPM
$9/2_1^- \rightarrow 7/2_1^-$	0.5776	0.0335	100	100
$11/2_1^- \rightarrow 9/2_1^-$	0.5691	0.0664	79	61
$\rightarrow 7/2_1^-$	0.1346		21	39
$13/2_1^- \rightarrow 11/2_1^-$	0.4787	0.0933	60	43
$\rightarrow 9/2_1^-$	0.2489		40	57
$15/2_1^- \rightarrow 13/2_1^-$	0.3807	0.1258	41	30
$\rightarrow 11/2_1^-$	0.3332		59	70
$17/2_1^- \rightarrow 15/2_1^-$	0.3053	0.1352	41	28
$\rightarrow 13/2_1^-$	0.3923		59	72
$19/2_1^- \rightarrow 17/2_1^-$	0.2423	0.1769	21	18
$\rightarrow 15/2_1^-$	0.4353		79	82
$21/2_1^- \rightarrow 19/2_1^-$	0.1960	0.1510	31	21
$\rightarrow 17/2_1^-$	0.4620		69	79
$23/2_1^- \rightarrow 21/2_1^-$	0.1545	0.2230	15	12
$\rightarrow 19/2_1^-$	0.4847		85	88
$25/2_1^- \rightarrow 23/2_1^-$	0.1254	0.1386	29	16
$\rightarrow 21/2_1^-$	0.4897		71	84
$27/2_1^- \rightarrow 25/2_1^-$	0.0962	0.2649	17	9
$\rightarrow 23/2_1^-$	0.5007		83	91
$29/2_1^- \rightarrow 27/2_1^-$	0.0001	0.0002	34	20
$\rightarrow 25/2_1^-$	0.0005		66	80
$31/2_1^- \rightarrow 29/2_1^-$	0.0175	0.2163	24	79
$\rightarrow 27/2_1^-$	0.0117		76	20
$33/2_1^- \rightarrow 31/2_1^-$	0.0153	0.0503	30	9
$\rightarrow 29/2_1^-$	0.3687		70	91
$35/2_1^- \rightarrow 33/2_1^-$	0.0273	0.4005	21	23
$\rightarrow 31/2_1^-$	0.4690		79	77
$37/2_1^- \rightarrow 35/2_1^-$	0.0222	0.0619	23	7
$\rightarrow 33/2_1^-$	0.4080		77	93
$39/2_1^- \rightarrow 37/2_1^-$	0.0325	0.5181	31	24
$\rightarrow 35/2_1^-$	0.4694		69	76
$41/2_1^- \rightarrow 37/2_1^-$	0.4259		100	100
$43/2_1^- \rightarrow 41/2_1^-$	0.0285	0.5254		20
$\rightarrow 39/2_1^-$	0.4684		100	80
$45/2_1^- \rightarrow 41/2_1^-$	0.4191		100	100
$47/2_1^- \rightarrow 45/2_1^-$	0.0226	0.4899		15
$\rightarrow 43/2_1^-$	0.4563		100	85
$49/2_1^- \rightarrow 45/2_1^-$	0.3939		100	100
$51/2_1^- \rightarrow 49/2_1^-$	0.0172	0.4470		11
$\rightarrow 47/2_1^-$	0.4331		100	89

Table 2. (Continued).

Transition	IBFBPM		I_γ	
	$B(E2)$ (e^2b^2)	$B(M1)$ (μ_N^2)	Exp.	IBFBPM
$7/2_2^+ \to 5/2_2^+$	0.2126	0.0649	100	100
$9/2_2^+ \to 7/2_3^+$	0.0029	0.0542		20
$\to 7/2_2^+$	0.5739	0.0582	74	57
$\to 5/2_2^+$	0.0654		26	23
$11/2_2^+ \to 9/2_2^+$	0.5065	0.0869	40	44
$\to 7/2_3^+$	0.0046		15	1
$\to 7/2_2^+$	0.1909		45	55
$13/2_2^+ \to 11/2_2^+$	0.4075	0.0845	38	21
$\to 11/2_3^+$	0.0124	0.0795		21
$\to 9/2_2^+$	0.2899		62	59
$15/2_2^+ \to 13/2_2^+$	0.3172	0.1176	25	24
$\to 11/2_2^+$	0.3625		75	76
$17/2_2^+ \to 15/2_2^+$	0.2492	0.0866	17	11
$\to 15/2_3^+$	0.0187	0.1026		20
$\to 13/2_2^+$	0.3981		83	69
$19/2_2^+ \to 17/2_2^+$	0.1822	0.1255	24	15
$\to 15/2_2^+$	0.4315		76	79
$\to 15/2_3^+$	0.0183			6
$21/2_2^+ \to 19/2_2^+$	0.1430	0.0611	22	5
$\to 19/2_3^+$	0.0323	0.1426		24
$\to 17/2_2^+$	0.4383		78	71
$23/2_2^+ \to 21/2_2^+$	0.0816	0.0801	25	5
$\to 19/2_2^+$	0.0674		75	8
$\to 19/2_3^+$	0.3868			87
$25/2_2^+ \to 23/2_2^+$	0.0703	0.2090	16	15
$\to 21/2_2^+$	0.4406		84	85
$5/2_3^+ \to 5/2_2^+$	0.0030	0.0123		16
$\to 3/2_3^+$	0.0765	0.0320	66	66
$\to 1/2_3^+$	0.2750		34	18
$7/2_3^+ \to 5/2_3^+$	0.0140	0.0456	3	4
$\to 5/2_2^+$	0.0759	0.0167	6	60
$\to 3/2_3^+$	0.2792		91	36
$9/2_3^+ \to 7/2_3^+$	0.0132	0.0206	34	29
$\to 5/2_3^+$	0.4233		66	71
$11/2_3^+ \to 9/2_3^+$	0.0064	0.0563	< 0.5	2
$\to 7/2_3^+$	0.4353		76	98
$\to 7/2_2^+$	0.0004		24	0.2
$13/2_3^+ \to 11/2_3^+$	0.0060	0.0119	19	10
$\to 9/2_3^+$	0.4722		81	90
$15/2_3^+ \to 13/2_2^+$	0.0188	0.0047	3	0.7
$\to 11/2_2^+$	0.0004		10	0.1
$\to 11/2_3^+$	0.4934		87	99

Table 2. (Continued).

Transition	IBFBPM		I_γ	
	$B(E2)$ (e^2b^2)	$B(M1)$ (μ_N^2)	Exp.	IBFBPM
$17/2_3^+ \rightarrow 15/2_2^+$	0.0112	0.0130		10
$\rightarrow 15/2_3^+$	0.0113	0.0711	7	82
$\rightarrow 13/2_3^+$	0.0186		93	8
$\rightarrow 13/2_2^+$	0.0003			
$19/2_3^+ \rightarrow 15/2_3^+$	0.4879		100	100
$21/2_3^+ \rightarrow 19/2_3^+$	0.0019	0.0822		27
$\rightarrow 17/2_3^+$	0.4450		100	73
$23/2_3^+ \rightarrow 21/2_2^+$	0.0631	0.0767		4
$\rightarrow 19/2_2^+$	0.4014			63
$\rightarrow 19/2_3^+$	0.0948		100	33
$25/2_3^+ \rightarrow 21/2_3^+$	0.0019		100	93
$\rightarrow 21/2_2^+$	0.00008			7
$27/2_3^+ \rightarrow 25/2_3^+$	0.0638	0.0378		70
$\rightarrow 23/2_3^+$	0.0009		100	30
$29/2_3^+ \rightarrow 25/2_3^+$	0.2724		100	100
$31/2_3^+ \rightarrow 27/2_3^+$	0.4173		100	100
$33/2_3^+ \rightarrow 31/2_3^+$	0.0645	0.0057		9
$\rightarrow 29/2_3^+$	0.4103		100	91
$35/2_3^+ \rightarrow 31/2_3^+$	0.2921		100	100
$37/2_3^+ \rightarrow 33/2_3^+$	0.3388		100	82
$\rightarrow 35/2_3^+$	0.0011	0.0355		18
$39/2_3^+ \rightarrow 35/2_3^+$	0.4352		100	100
$43/2_3^+ \rightarrow 39/2_3^+$	0.4180		100	100
$41/2_3^+ \rightarrow 37/2_3^+$	0.1079		100	53
$\rightarrow 39/2_3^+$	0.0240	0.0205		47
$47/2_3^+ \rightarrow 43/2_3^+$	0.3764		100	100
$51/2_3^+ \rightarrow 47/2_3^+$	0.3234		100	100

yrast sequence corresponds to the collective $SU(3)$-$O(6)$ ground-state band. Between $I = 10^+$ and $I = 12^+$ a band based on the $(\pi h_{11/2})^2$ configuration enters the yrast line. For $12^+ \leq I \leq 22^+$ the yrast states are based on the two-proton configuration $(\pi h_{11/2})^2$ coupled to the ground-state band of the boson core. Close above the yrast the model predicts the lowest band based on the $(\nu h_{11/2})^2$ configuration. Although not observed in the present experiment, the forking of the ground-state band into two S-bands, one proton and one neutron, is a common feature in light Ce, Ba and Xe nuclei [25]. The present calculation, performed in the laboratory frame, agrees with the description of the forking mechanism in the cranking framework [25]. The band $(\nu h_{11/2})^2$, as well as the low-spin part of the γ-band has also been observed in ^{126}Ce [22]. In fig. 4 we include the theoretical prediction for the position of the γ-band.

The strength parameters of the boson-fermion interaction [19] are (all values in MeV): $A_0^\pi = 0.006$, $\Gamma_0^\pi = 0.1$, $\Lambda_0^\pi = 6.0$, $A_0^\nu = 0$, $\Gamma_0^\nu = 0.5$, $\Lambda_0^\nu = 1.85$ for states of positive parity in ^{125}Ce, and $A_0^\pi = 0.04$, $\Gamma_0^\pi = 0.25$, $\Lambda_0^\pi = 11.0$, $A_0^\nu = 0.08$, $\Gamma_0^\nu = 0.4$, $\Lambda_0^\nu = 1.3$ for negative-parity states.

The boson operator of the dynamical proton fermion-boson interaction contains the additional term

$$\eta \sum_{L_1 L_2} \left[\left(d^\dagger \times \tilde{d} \right)^{(L_1)} \left(d^\dagger \times \tilde{d} \right)^{(L_2)} \right]^{(2)}$$

introduced in ref. [26]. In the present calculation, $\eta^\pi = 0$ for positive-parity states and $\eta^\pi = 0.3$ for negative-parity states.

The values of the strength parameters of the fermion-boson interactions are somewhat different from the ones used in a recent analysis of Pr nuclei in ref. [21]. In the analysis of ref. [21] very limited information on the level spectrum of ^{125}Ce was used to determine the neutron fermion-boson interaction strengths. Based on new experimental data on ^{125}Ce, these parameters have been determined much more accurately in the present calculation.

The strength parameter of the pair-breaking interaction is $U_2 = 0.25$ MeV, both for proton pairs and neutron pairs.

The calculations of positive- and negative-parity structures in ^{125}Ce are performed in the configuration space of one-neutron states and one-neutron plus two-proton states coupled to the collective boson states. The transition probabilities are calculated with the following set of effective charges and gyromagnetic ratios [21]: $e^{\pi} = 1.0$, $e^{\nu} = 0.5$, $e^{\rm vib} = 0.95$, $g_l^{\pi} = 1.0$, $g_s^{\pi} = 0.5\ g_s^{\pi,\rm free} = 2.793$, $g_l^{\nu} = 0$, $g_s^{\nu} = 0.5\ g_s^{\nu,\rm free} = -1.913$, $g_{\rm R} = \frac{Z}{A} = 0.464$.

In fig. 5 the calculated negative-parity states are compared with the experimental band 1. This band is based on the $\nu h_{11/2}$ orbital for the states with $I \leq 27/2^-$, and on the three-fermion configuration $\nu h_{11/2}\ (\pi h_{11/2})^2$ for $I \geq 29/2^-$. The structure of this band is very simple. The neutron $\nu h_{11/2}$ orbital couples to the yrast sequence of states in the core nucleus ^{124}Ce (fig. 4). The calculated excitation energies are in excellent agreement with experimental data.

The positive-parity states of ^{125}Ce are displayed in fig. 6 in comparison with the experimental bands. Band 2 is based on the $\nu d_{5/2}$ and $\nu g_{7/2}$ neutron orbitals. Band 3, in addition, contains sizeable components based on the $\nu d_{3/2}$ and $\nu s_{1/2}$ states. While the alignment of a proton pair is not observed in band 2, the states with $I \geq 25/2^+$ of band 3 are based on the one-neutron plus $(\pi h_{11/2})^2$ configuration. The calculation nicely reproduces the observed structure of these bands. In fact, also in our calculation band 2 cannot be extended above $I > 25/2^+$. The wave functions of the calculated states are strongly fragmented, and one cannot identify the possible high-spin members of this band.

In table 2 we include the calculated $B(E2)$ and $B(M1)$ values for the transitions observed in experiment, and compare the transition intensities with the experimental values. A very good agreement is found between theory and experiment for transitions between states of negative parity. For the positive-parity sequences the agreement is fair for the low-spin part of the spectrum, as well as for the transitions between states with $I > 25/2^+$. The wave functions of the calculated states between $17/2^+$ and $23/2^+$ are strongly fragmented, and this is reflected in very strong inter-band transitions, in contrast with experimental data. We also notice the very weak transitions in the regions of band crossings. This is characteristic for the interacting boson plus broken-pairs models, and reflects the weak mixing between states with different number of broken pairs [27,28].

5 Conclusions

The level scheme of the odd-even nucleus ^{125}Ce has been studied in detail. Two new bands were identified and the previously known structures were extended to higher spins. The observed level structure have been discussed in the framework of the IBFM plus broken-pairs model. Good agreement is found between theory and experiment for both parities, apart for the band crossing region in the positive-parity band 3, where the intensity ratio between the in-band and inter-band transitions is in contrast with experimental data.

References

1. C. Rossi Alvarez, Nucl. Phys. News, Vol. **3**, no. 3 (1993).
2. E.S. Paul, A.J. Boston, A. Galindo-Uribarri, T.N. Ginter, C.J. Gross, A.N. James, P.J. Nolan, R.D. Page, S.D. Paul, A. Piechaczek, D.C. Radford, W. Reviol, L.L. Riedinger, H.C. Scraggs, W. Weintraub, C.-H. Yu, Phys. Rev. C **58**, 801 (1998).
3. P.A. Wilmarth, J.M. Nitschke, R.B. Firestone, J. Gilat, Z. Phys. A **325**, 485 (1986).
4. A. Osa, M. Asai, M. Koizumi, T. Sekine, S. Ichikawa, Y. Kojima, H. Yamamoto, K. Kawade, Nucl. Phys. A **588**, 185c (1995).
5. B.M. Nyako, J. Gizon, V. Barci, A. Gizon, S. André, D. Barnéoud, D. Curien, J. Genevey, J.C. Merdinger, Z. Phys. A **334**, 513 (1989).
6. A. Gizon, J. Genevey, D. Barnéoud, A. Astier, R. Béraud, Gh. Cata-Danil, A. Emsallem, J. Gizon, Y. Le Coz, C.F. Liang, P. Paris, Z. Phys. A **351**, 361 (1995).
7. A. Gizon, J. Genevey, D. Bucurescu, Gh. Cata-Danil, J. Gizon, J. Inchaouh, D. Barnéoud, T. von Egidy, C.F. Liang, B.M. Nyako, P. Paris, I. Penev, A. Plochocki, E. Ruchowska, C.A. Ur, B. Weiss, L. Zolnai, Nucl. Phys. A **605**, 301 (1996).
8. R. Ma, E.S. Paul, C.W. Beausang, S. Shi, N. Xu, D.B. Fossan, Phys. Rev. C **36**, 2322 (1987).
9. E. Farnea, G. de Angelis, D. De Acuna, A. Gadea, D.R. Napoli, P. Spolaore, A. Buscemi, R. Zanon, R. Isocrate, D. Bazzacco, C. Rossi Alvarez, P. Pavan, A.M. Bizzetti-Sona, P.G. Bizzetti, Nucl. Instrum. Methods Phys. Res. A **400**, 87 (1997).
10. C.M. Petrache, D. Bazzacco, S. Lunardi, C. Rossi Alvarez, G. de Angelis, M. De Poli, D. Bucurescu, C.A. Ur, P.B. Semmes, R. Wyss, Nucl. Phys. A **597**, 106 (1996).
11. C.M. Petrache, D. Bazzacco, P. Bednarczyk, G. de Angelis, M. De Poli, C. Fahlander, G. Falconi, E. Farnea, A. Gadea, M. Lunardon, S. Lunardi, N. Marginean, R. Menegazzo, P. Pavan, Zs. Podolyak, C. Rossi Alvarez, C.A. Ur, R. Venturelli, L.H. Zhu, R. Wyss, Phys. Lett. B **415**, 223 (1997).
12. F. Iachello, D. Vretenar, Phys. Rev. C **43**, 945 (1991).
13. D. Vretenar, G. Bonsignori, M. Savoia, Phys. Rev. C **47**, 2019 (1993).
14. D. Vretenar, G. Bonsignori, M. Savoia, Z. Phys. A **351**, 289 (1995).
15. D. Vretenar, S. Brant, G. Bonsignori, L. Corradini, C.M. Petrache, Phys. Rev. C **57**, 675 (1998).
16. A. Arima, F. Iachello, Phys. Rev. Lett. **35**, 1069 (1975).
17. F. Iachello, A. Arima, *The Interacting Boson Model* (Cambridge University Press, Cambridge, 1987).
18. F. Iachello, O. Scholten, Phys. Rev. Lett. **43**, 679 (1979).
19. F. Iachello, P. Van Isacker, *The Interacting Boson-Fermion Model* (Cambridge University Press, Cambridge, 1991).
20. C.M. Petrache *et al.*, to be published.
21. C.M. Petrache, M. Nespolo, S. Brant, G. Lo Bianco, D. Bazzacco, S. Lunardi, P. Spolaore, M. Axiotis, N. Blasi, G. de Angelis, T. Kröll, N. Marginean, T. Martinez, R. Menegazzo, D.R. Napoli, B. Quintana, A. Saltarelli, A. Ventura, D. Vretenar, Phys. Rev. C **64**, 044303 (2001).
22. C.M. Petrache *et al.*, to be published.

23. L.S. Kisslinger, R.A. Sorensen, Rev. Mod. Phys. **35**, 853 (1963).
24. Gh. Cata-Danil, D. Bucurescu, A. Gizon, J. Gizon, J. Phys. G **20**, 1051 (1994).
25. R. Wyss, A. Grandearth, R. Bengtsson, P. von Brentano, A. Dewald, A. Gelberg, A. Gizon, J. Gizon, S. Harissopulos, A. Johnson, W. Lieberz, W. Nazarewicz, J. Nyberg, K. Schiffer, Nucl. Phys. A **505**, 337 (1989).
26. C.M. Petrache, R. Venturelli, D. Vretenar, D. Bazzacco, G. Bonsignori, S. Brant, S. Lunardi, N.H. Medina, M.A. Rizzutto, C. Rossi Alvarez, G. de Angelis, M. De Poli, D.R. Napoli, Nucl. Phys. A **617**, 228 (1997).
27. D. Vretenar, V. Paar, G. Bonsignori, M. Savoia, Phys. Rev. C **42**, 993 (1990).
28. D. Vretenar, V. Paar, G. Bonsignori, M. Savoia, Phys. Rev. C **44**, 223 (1991).